CNRS
Centre National de la Recherche Scientifique

INFN
Instituto Nazionale di Fisica Nucleare

Timing calibration during VSR1

A. Masserot, B. Mours, L. Rolland

VIR-028A-08

May 5, 2008

VIRGO * A joint CNRS-INFN Project
Project office: Traversa H di via Macerata - I-56021 S. Stefano a Macerata, Cascina (PI)
Secretariat: Telephone (39) 50 752 521 – Fax (39) 50 752 550 – e-mail virgo@pisa.infn.it

Contents

L

1 Introduction

In order to make multi-detector coincidences, the absolute time of the detector data must be known. After a brief overview of the timing system [1], the absolute timing of the Virgo data is estimated.

In order to get a good accuracy of the h(t) reconstruction, the delays from the longitudinal correction signals applied to the mirror and marionnette actuators and the dark fringe must be set within a few μs. Delays of the order of 450 μs have been measured through the actuator calibration main stream [2] from the control signal Sc_ $*$ _zCorr to the dark fringe signal Pr_B1_ACp. In this note, we consider the processing of the signals in order to explain such delays and estimate possible systematic errors.

Finally, some checks about the stability of the Virgo timing system are described.

2 Virgo timing system overview

The Virgo timing system is based on a master timing system controlled by GPS. Its roles are to give the rythm of the control loops and to give the time stamps to the acquisition system (DAQ).

The GPS receiver delivers a 5 MHz signal to the master timing board. The master timing board then builds four signals which are then distributed through optical fibers to the different buildings in order to control loop frequencies and to give the time to the acquisition system:

- a *fast clock* signal (2.5 MHz),
- a sampling signal at 20 kHz to sample the rapid signals,
- a *frame signal* at 1 Hz to define the frame limits,
- a signal at 1/32768 Hz (or triggered by the user) to define the "run" limits. It is used to synchronize the frame numbers.

A quartz oscillator is set on the GPS board, with a relative stability of $\sim 10^{-6}$. However, the frequency of this oscillator is enslaved on the GPS time: corrections of the time and of the frequency are applied as function of the GPS system information. Deviations of the output time with the GPS time are less than 1 μs.

A few microseconds $t_1 \sim 3\,\mu$s delay is expected between the clock from the GPS receiver and the *frame* signal from the timing system. To monitor it, the 1 Hz *frame* signal is sent back to the GPS receiver in order to measure its delay from the beginning of the last second in the GPS. This delay is stored in the Virgo data in the channel TiM_GTimeN (in ns). It can

change when the timing system is restarted or when the GPS encounter problems (for example, a temporary loss of satellites).

The four output signals from the master timing system are delivered to the timing distribution boards of the different buildings. They are first converted to optical signals and sent through silica optical fibers with refraction index of the order of 1.5. In order to have the same propagation delays for all buildings, all the optical fibers have the same length ($3350 \pm 100\,\mathrm{m}$). The expected propagation delay is of the order of $t_p = 16.8 \pm 1\,\mu\mathrm{s}$. The optical signals are then converted to electrical signals, distributed from the timing distribution boards to the user crates and used to control the rate of the different processes.

From every building, the local distribution boards send back the 20 kHz and 1 Hz clock signals to the control part of the master timing board. The signals are compared to the clock of a second GPS receiver. The total delay between the propagated clock signals and the initial clock signals from the master timing board is stored in four channels TiM_rtt$(1, 2, 3, 4)$ (in ns) corresponding to the four buildings returned signals. The four delays are expected to be the same and of the order of $t_2 = 2 \times t_p = 33.6 \pm 2\,\mu\mathrm{s}$.

3 Absolute timing of the Virgo data

Specific data have been taken in April 2008 in order to check our understanding of the timing delays and estimate the systematic error on the absolute timing of the Virgo data.

The absolute timing during VSR1 is then estimated.

3.1 Estimation of the systematic error

Measurements to characterize the Virgo absolute timing have been performed during the night from 7th to 8th April 2008. They are analysed in the following paragraphs.

3.1.1 Estimation of the propagation time of the clock signals

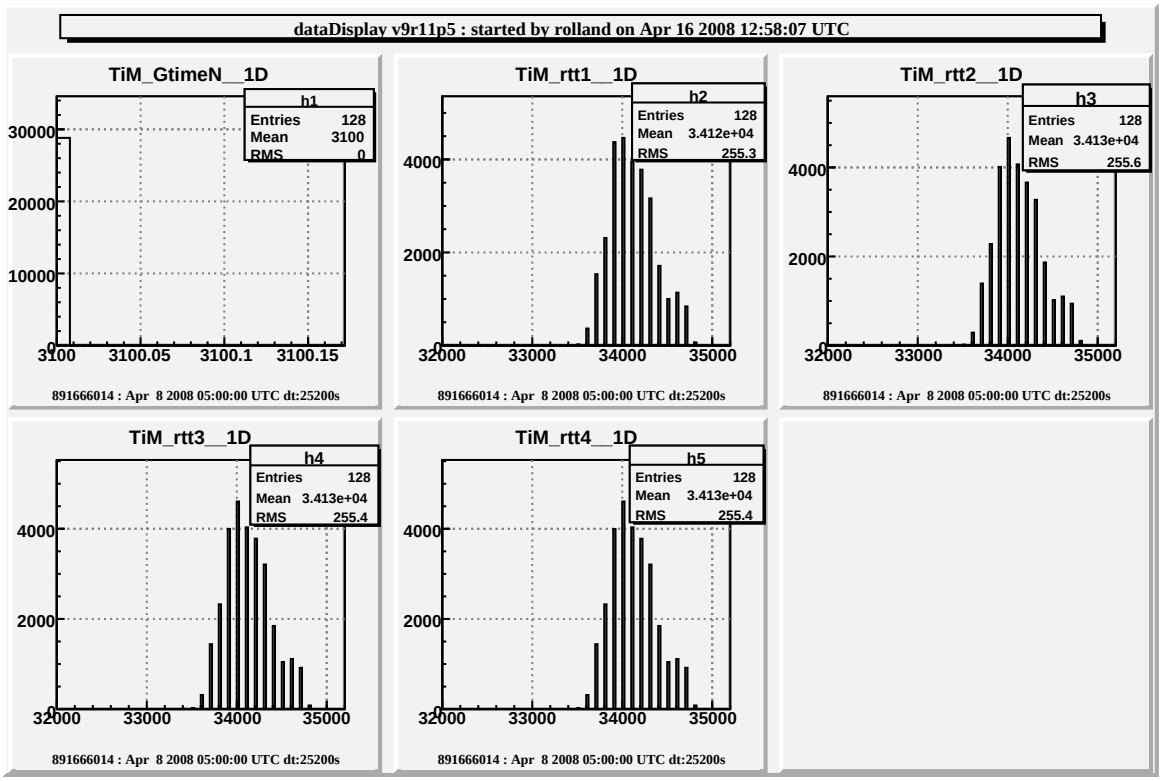

Figure 1: ***Distribution of the timing monitoring signals*** *during the night from 7th to 8th April 2008. The unit of the channels are ns.*

On April 8th 2008, the delay between the GPS receiver and the clocks from the master timing board, measured in the channel TiM_GTimeN, was $t_1 = 3.1\,\mu$s (figure 1). The propagation delay from the master timing clock and the second GPS receiver, measured though the channels TiM_rtt$(1, 2, 3, 4)$ was $t_2 = 34.1\,\mu$s, with a RMS of 255 ns. From this measurements, the

propagation time from the master timing board to the timing distribution boards is estimated to $t_p = 17.1\,\mu$s. This is in agreement with the expected propagation time delay within $0.3\,\mu$s. For this night, the expected delay of the Virgo data related to the GPS time is thus estimated to be $t_1 + t_p = 20.2\,\mu$s.

3.1.2 Estimation of the frame time delay from the GPS time

The 1 PPS signal from the master timing GPS receiver has been sent to an ADC of the dark fringe photodiode readout in the central building and stored in the data through the DAQ. This allows to measured the delay between the rising-edge of the 1 PPS signal, giving the absolute beginning of a second, and the first sample of the frame. The frames are defined such that the first sample is at a time with an integer number of seconds. This delay thus gives the absolute delay of the Virgo data.

In practice, the 1 PPS output is a 500 ms rectangular signal. The rising edge of the signal is detected by a flip-flop which rapidly triggers the integration of a reference signal. The signal is integrated up to a given value and the output of the integrator is reset to 0. The ramp is digitized through a 4-channels ADC (without anti-alias filter) and stored into the frames. An example of such a signal[1] is shown in the figure 2(a). The time of the rising-edge of the GPS signal is given by the time of the beginning of the ramp. This one can be adjusted fitting a line on the whole ramp.

Such data have been taken during the night from 7th to 8th April 2008. Every ramps (stored in the channel Pr_TiPulse) have been adjusted by a line. The offset between the initial time of the ramp t_0, giving the time of the GPS pulse, and the time of the frame starting just after have been calculated. Its distribution is given in the figure 2(b). An average offset of 22.3 μs with RMS of 83 ns is found.

3.1.3 Virgo absolute timing and systematic error

Two measurements of the absolute delay between the Virgo time stored in the frames and the GPS time during the night from 7th to 8th April 2008 give $20.2\,\mu$s and 22.3 μs respectively. For multi-detector analysis, the Virgo signals must thus be corrected for a 21 μs delay. Yet, $\sim 2\mu$s systematic errors have to be taken into account in the absolute timing of h(t).

3.2 Absolute timing during VSR1

The first method described above to measure the propagation time of the clock signals can be applied on the VSR1 data since the timing signals were monitored.

[1] In the plots to be fitted, the ith sample of the FrVect v, with value $v->dataD[i]$ is set at the time of the clock: $v->startX[0] + i \times v->dx[0]$.

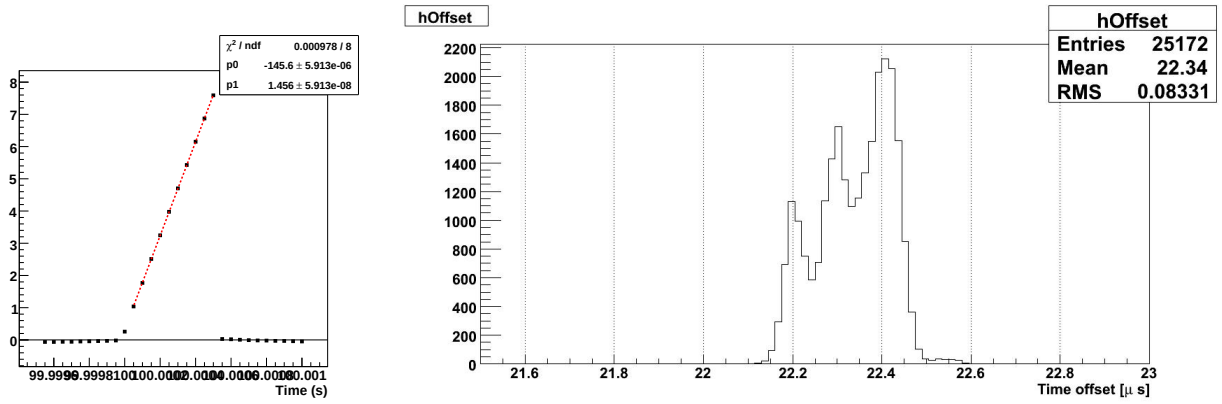

(a) Example of triangular signal.

(b) Absolute time delay distribution.

Figure 2: ***Example of triangular signal built from the GPS 1 PPS signal.***

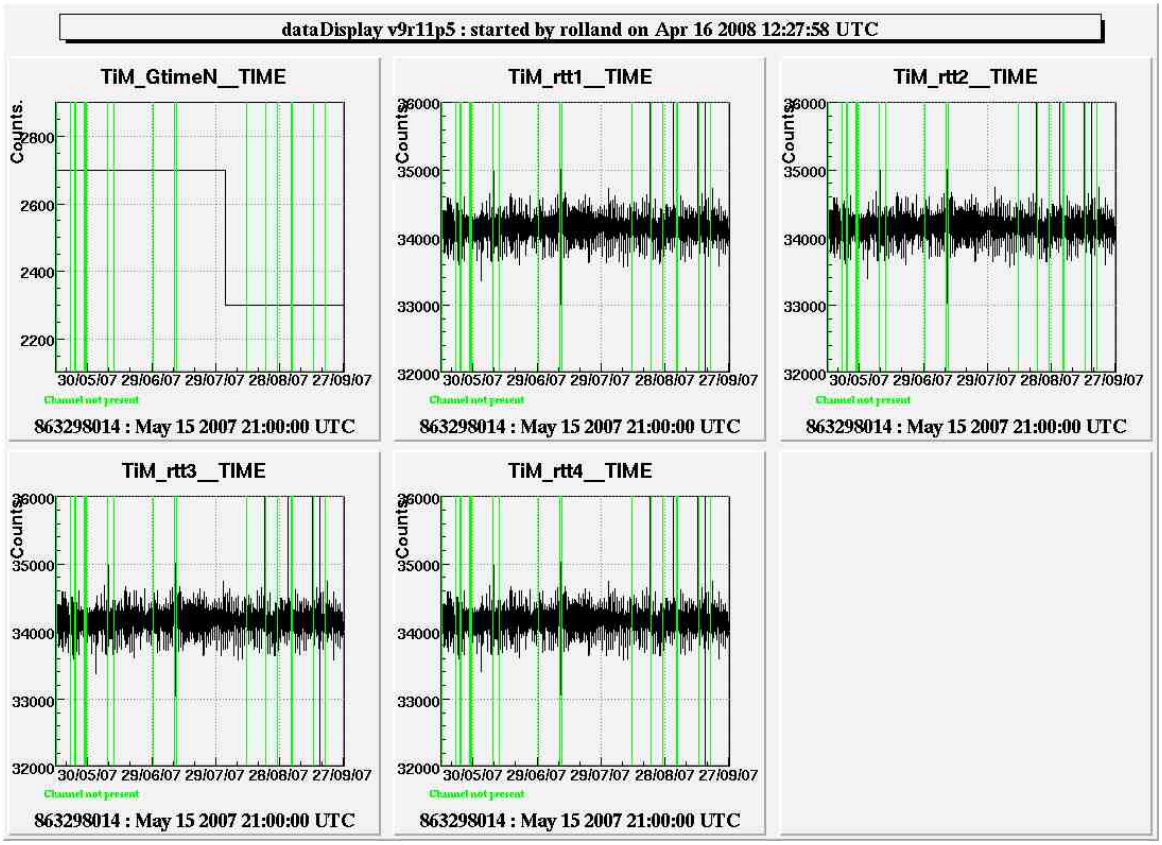

Figure 3: ***Master timing monitoring signals vs time during VSR1.***

The timing monitoring signals as function of time during VSR1 are shown on the figure 3. The delay measured by TiM_GTimeN changed on August 3rd 2007, around 14h18m42s UTC. It was $t_1 = 2.7\,\mu$s up to GPS 870185936, and then $t_1 = 2.3\,\mu$s from GPS 870185936. The variation of $0.4\,\mu$s is much lower than the estimated systematic errors and can be neglected in the following.

The return-time monitoring signals TiM_rtt$(1, 2, 3, 4)$ were constant during VSR1, with an average of $t_2 = 34.15\,\mu$s and a negligible RMS of $0.26\,\mu$s.

From these measurements, the absolute delay during VSR1 is $2.7 + 17.1 = 20.8\,\mu$s. It is compatible with the measurements described in previous section.

The h(t) reconstructed using the VSR1 data should thus be corrected for a $21\,\mu$s delay. Then, the systematic errors on the absolute timing of h(t) are estimated to $2\,\mu$s.

4 Timing delay from the actuation to the dark fringe

In this section, the details of the signal processing from the mirror actuation input to the dark fringe output are given. The delay of the processing is estimated to check our understanding of the delay found by the calibration stream.

The signal processing is made of the following pieces:

- the mirror actuation, from Sc_ $*$ _zCorr to the force applied on the mirror. It depends on the mode of the suspension: High Power (HP) or Low Noise (LN).
- the propagation time of the mirror deformation from the magnets to the mirror centre.
- the mechanical response of the pendulum.
- the optical response of the interferometer. It is different between the data in free swinging Michelson configuration and the data in Science Mode.
- the sensing of the dark fringe, from the power on the photodiodes to the Pr_B1_ACp signal.

In the following, the way a digital electronic signal is stored into the DAQ frames is detailed for both the actuation part and the dark fringe sensing. The figures are made around the time of the beginning of a new frame.

4.1 Signal processing in the actuation part

From the channel Sc_ $*$ _zCorr to the force on the mirror, the signal goes through the following path:

- the DSP of the coil actuation,
- the DAC of the coil actuation, with its anti-image filter.
- the coil and serie resistors. They can be modeled with a pole whose value depends on the HP or LN mode of the suspension.

The way the signal goes through this path and is stored in the DAQ is described in order to estimate the expected delay from the recorded channel Sc_ $*$ _zCorr to the force applied on the mirror. The value is then compared to measurements.

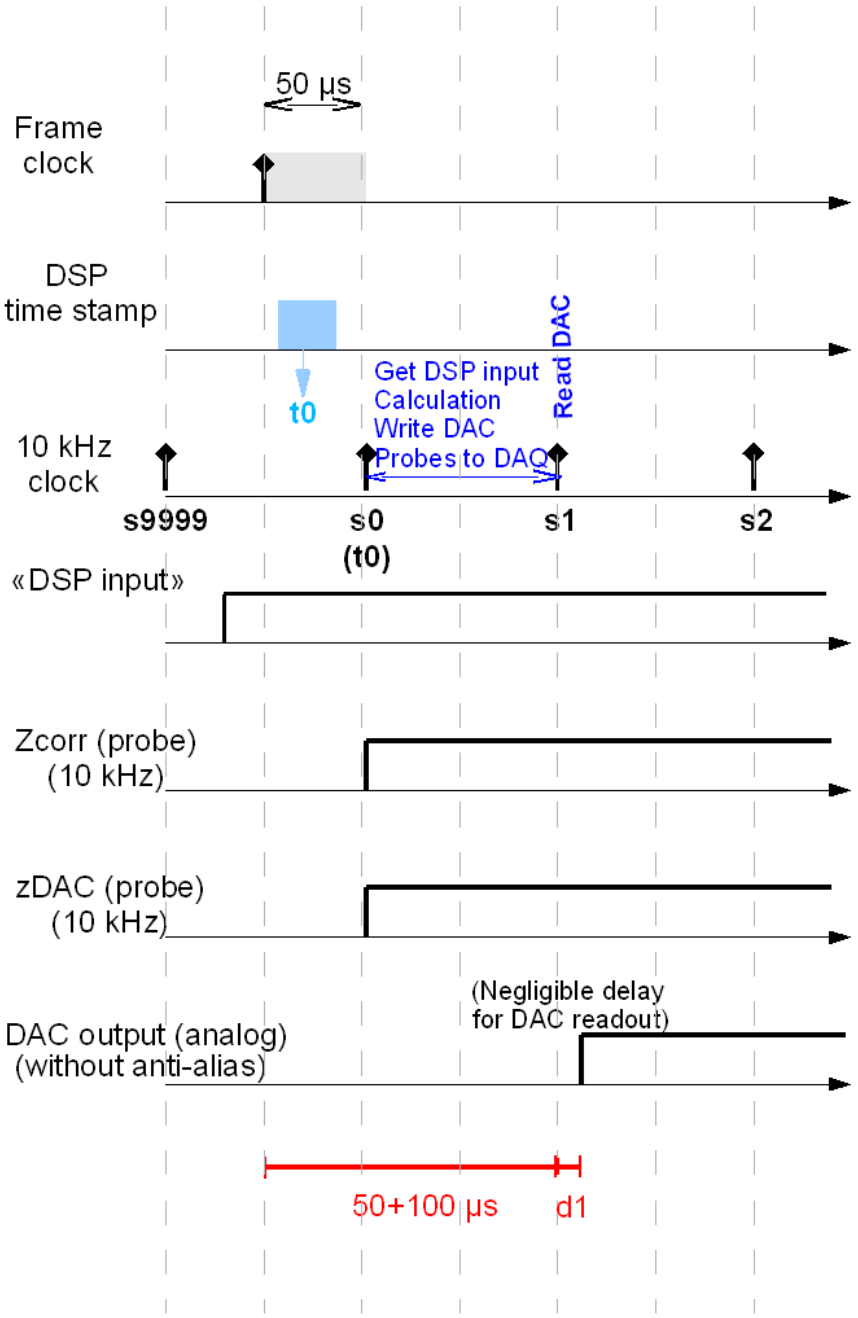

Figure 4: ***Signal processing in the actuation part.*** *See text for details.*

4.1.1 Expected delay

The signal processing is shown on the figure 4.

The *frame signal* is a serie of one 50 μs-pulse per second. The DSP signals are sampled with a frequency of 10 kHz. The 10 kHz clock is set such that the *frame* pulse is in-between two 10 kHz-clock pulses. For a 10 kHz time serie, the first sample s_0 contains the value computed between the impulses s_0 and s_1. It is offset from the beginning of the frame by 50 μs.

The ith DSP cycle (i from 1 to 10000) starts and ends with two consecutive 10 kHz clock pulses: s_{i-1} and s_i. In practice, it starts 7 μs after the pulse, but this is not visible in the data stored by the DAQ. During the first cycle (from s_0 to s_1), the DSP gets the input values, makes calculations, writes the output values to the DAC and sends the probed output to the DAQ with the flag of sample s_0. Assuming a DSP input (see figure), its value is thus processes by the DSP when it receives the 10 kHz-pulse s_0. After the calculation, the probed values of $Sc\_ * \_zCorr$ and $Sc\_ * \_zDAC$ (value written in the DAC) are stored in the DAQ in the sample s_0. The DAC readout is triggered by the 10 kHz clock pulses and the corresponding values are thus settled at sample s_1 (this does not take into account the additional delay of the DAC anti-image filter). For frequencies lower than ~ 1 kHz, the phase of the DAC anti-image filter is equivalent to a delay of 180 μs. An additionnal delay of 0.350 μs is expected between the time the DAC is triggered and the time the DAC data are available at the analog output (DAC settling time).

The current flowing in the coil is then filtered by the simple pole[2] made of the coil ($L \sim 3 \times 10^{-3}$ H) and the serie resistors ($\sim 50\,\Omega$ in HP mode and $\sim 6\,k\Omega$ in LN mode for the cavity mirrors, $\sim 1\,k\Omega$ in LN mode for the BS mirror). The equivalent delays d_{coil} below the pole frequencies are 60 μs and 0.5 μs (3 μs for BS) respectively.

The total delay between the $Sc\_ * \_zCorr$ stored signal and the force applied on a mirror is thus $\sim 330.4 + d_{coil}$ μs. For an end mirror in LN mode, the ~ 330.9 μs delay is coming from:

- 50 μs between the beginning of the frame and the first 10 kHz sample,
- 100 μs since $Sc\_ * \_zCorr$ is stored by the DAQ in the sample s_{i-1} and the DAC is triggered by the clock pulse s_i,
- 0.350 μs to settle the DAC,
- 180 μs from the DAC anti-image.
- 0.5 μs from the coil and serie resistors.

The expected delay is thus ~ 390.4 μs for the end mirror actuation in HP mode and ~ 333.4 μs for the BS mirror actuation.

[2] The pole frequency is defined as $R/(2\pi L)$.

In LN mode, there are emphasis filters in the DSP to compensate the de-emphasis filters set in the coil driver. This should not induce any phase effect between Sc_*_zCorr and the signals after the coil current.

In the calibration stream, the mirror actuation TFs have been corrected for the mechanical response of the pendulum. The phase from the pendulum response should not be taken into accoun in this analysis but should be corrected for in the h-reconstruction.

4.1.2 Measurements of the delay

It is possible to measure the current flowing in the coils using the channels $Ca\_*\_RM\_Coil\{U,D\}$ in order to check the expected delay. This channel is sampled at 20 kHz through a shaping filter with a zero and a pole at 3 and 97 Hz. The sample time is corrected for the 16-channels ADC anti-alias filter delay ($\sim 1.7\,$ms) in the DAQ. The 20 kHz sampled channels are not offset from the beginning of the frame. The channels $Ca\_*\_RM\_Coil\{U,D\}$ should thus be in phase with the force applied on the mirror.

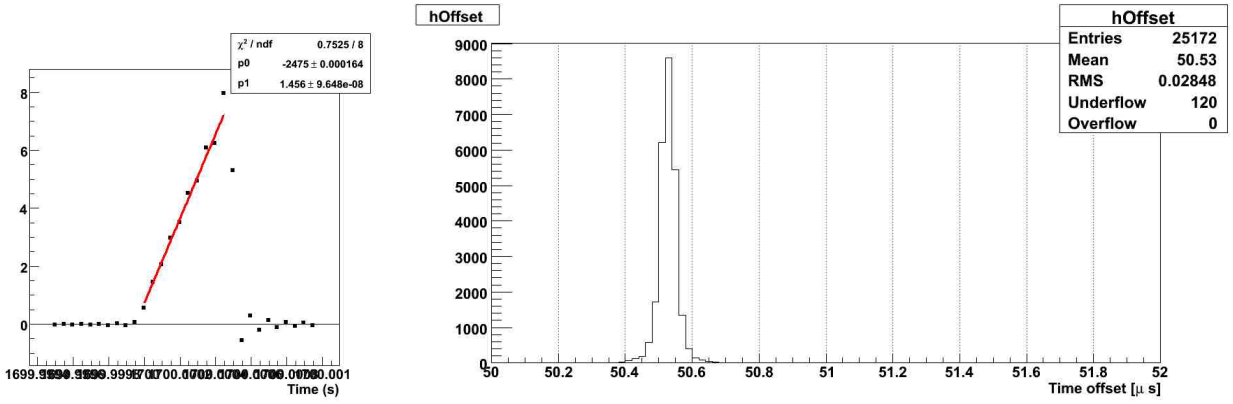

(a) Example of triangular signal in a 16-channel ADC.

(b) Absolute time delay distribution.

Figure 5: ***Example of triangular signal built from the GPS 1 PPS signal*** *and digitized through a 16-channels ADC with its anti-alias filter.*

In practice, the delay of anti-alias filter of the ADC channel is not perfectly corrected in the DAQ. In order to measure the error, the ramp generated from the 1 PPS signal from the GPS receiver has been sent to a 16-channels ADC. This is based on the same method as described in 3.1.2 (p. 5). The triangular signal is filtered by the ADC anti-alias filter, which induces systematic distorsion of the sampled ramp as shown in the figure 5(a). The distribution of the absolute time delay of the 16-channels ADC sampled signals to the GPS time is given in the figure 5(b). The delay is of the order of $50.5\,\mu$s. $21\,\mu$s are due to the delay of the Virgo absolute timing.

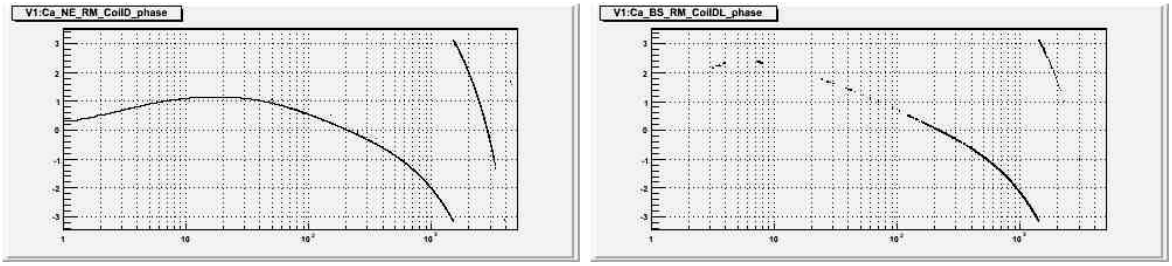

Figure 6: ***Phase (in radians) as function of frequency of the TF*** *Ca_ * _RM_Coil*/Sc_ * _zCorr for the NE, CoilD (left) and BS, CoilDL coils (right). The suspensions were in LN mode (GPS 875001614). Only the points with coherence higher than 99% are shown.*

	Tower	Coil	Minimum delay (μs)	Maximum delay (μs)	Average delay (μs)
LN mode	NE	CoilU	336	345	340
	NE	CoilD	336	345	340
	WE	CoilU	338	346	341
	WE	CoilD	337	345	340
	BS	CoilUL	318	328	322
	BS	CoilUR*	327	337	333
	BS	CoilDL	356	369	362
	BS	CoilDR	355	370	362
HP mode	NE	CoilU	406	421	411
	NE	CoilD	393	407	397
	WE	CoilU	388	417	402
	WE	CoilD	387	417	404
	BS	CoilUL	407	425	415
	BS	CoilUR*	411	430	418
	BS	CoilDL	411	427	419
	BS	CoilDR	408	427	416

Table 1: ***Minimum, maximum and average delay measured from the phase of the TF*** *Ca_ * _RM_Coil* **over** *Sc_ * _zCorr, after correction from the (3-97) Hz spaping filter. These delays include any delay from the coil current readout in the channels Ca_ * _RM_Coil*. The measured delays on data in LN mode and HP mode are given. Only the points with coherence higher than 99% between 500 Hz and 2 kHz were used. *: the phase has been shifted by $-\pi$. There must be a -1 sign in the current readout.*

The additionnal 29 μs are attributed to the bad compensation of the ADC anti-alias delay in the DAQ. It means that the channels $Ca\_*\_RM\_Coil\{U,D\}$ should thus be delayed by 29 μs compared to the other stored channels. Note that this error in the delay correction is 2% of the delay induced by the anti-alias filter. Since all the 16-channels ADC have the same digital anti-alias filter and the delay correction used in the DAQ is the same for all channels, the 29 μs delay should be the same for all channels (in particular for all the $Ca\_*\_RM\_Coil*$ channels).

The transfer functions (TF) of $Ca\_*\_RM\_Coil\{U,D\}$ over Sc_*_zCorr have been measured on VSR1 data in Science Mode from September 28th 2007 (GPS 875001614). The suspensions were in LN mode. The phase of the TF has been measured. An exemple is shown in the figure 6. After correction for the the 3-97 Hz shaping filter phase effect[3], the delay is computed for all points with coherence higher than 99% from 1 kHz to 2 kHz. The minimum, maximum and average delays measured for every mirror coils are given in the table 1. This delay should include the delay estimated in section 4.1.1 and the 29 μs delay from the 16-channels ADC used in the coil current readout. Examples of the residuals of the measured phase to the model including the shaping filter and a pure delay are shown in the figure 7. The residual errors on the delay are of the order of 4 μs.

[3] The equivalent delay due to the 3-97 Hz shaping filter is 59, 14.9 and 3.7 μs at 500 Hz, 1 kHz and 2 kHz respectively.

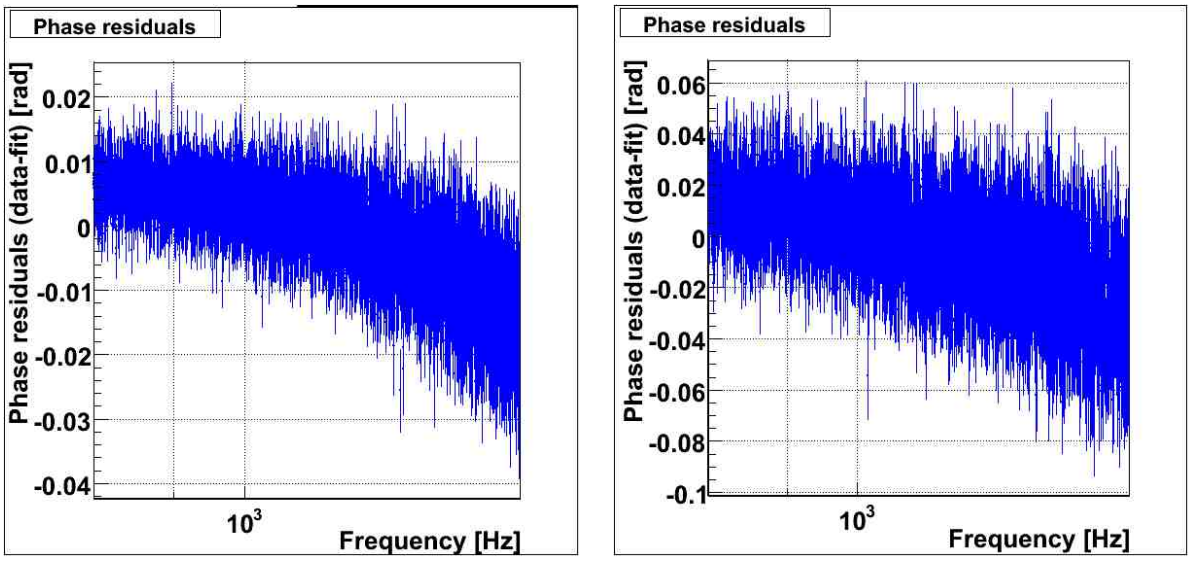

(a) NE coil U. (b) BS Coil DR.

Figure 7: ***Residuals of the phase of*** $Ca\_*\_RM\_Coil*$ ***to*** Sc$_*_$zCorr ***transfer function compared to a delay,*** *from 800 Hz to 1.5 kHz.*

Correcting for the readout delay, the measured delays from the Sc_ ∗ _zCorr channel to the force applied on the NE and WE mirrors with the actuation in LN mode, $340 - 29 = 311 \pm 4\,\mu$s, is lower than the expected $330.9\,\mu$s.

The measured delays for the NE and WE mirror actuation in HP mode (step4, September 28th 2007, GPS 875006584) are $60\,\mu$s higher than in LN mode, as expected due to the lower serie resistor values.

For the BS actuation, the expected delay is $\sim 333.4,\mu$s. The measurements described above give unexpected $\sim 40\,\mu$s different delays between the different coil actuation (from 291 to $331\,\mu$s). The values are about the expected one within $40\,\mu$s.

To conclude, the measured actuation delay is $20\,\mu$s lower than the expected delay for the end mirrors and $40\,\mu$s lower for the BS mirror. Since the origin of the difference is not understood, it could be in the actuation chain itself and not in the readout part of the $Ca\_ * \_RM\_Coil*$ channels. These numbers are thus an upper value of the systematic errors on the actuation timing.

4.2 Propagation of the mirror deformation to the mirror center

The actuation force is applied on the mirror at the level of the magnets. The mirror deformation then propagates to the center of the mirror at the speed of sound. The mirror motion is seen in the interferometer when the deformation reaches the main laser beam, at the center of the mirror. The beam radius being of the order of 3 cm, the deformation reaches the beam before the center of the mirror, reducing this delay.

The relevant characteristics of the mirrors [3] concerning the propagation of sound waves are given in the table 2. The speed of acoustic waves in silica is $5968\,\mathrm{m.s^{-1}}$ for longitudinal waves (and $3764\,\mathrm{m.s^{-1}}$ for transverse waves). The propagation times of the mirror deformation from the magnet position to the interferomater beam are thus estimated to be in the range $16 - 21\,\mu$s for the BS mirror and $25 - 30\,\mu$s for the cavity mirrors.

	BS	NI, WI	NE, WE
Material	SUPRASIL 311	SUPRASIL 312	HERASIL 1
Thickness e (mm)	55.0	96.8	95.7
Diameter D (mm)	230	350	350
Magnet position diameter d (mm)	215	305	305

Table 2: ***Mirror characteristics and magnet position.***

4.3 Optical response of the interferometer

Two configurations with different time of light travel in the arms have to be considered.

The measurements of the delay from Sc_ * _zCorr to Pr_B1_ACp are based on data in **free swinging Michelson** configurations. In these configurations, the light directly travels from the mirror to the dark fringe. The expected delay is thus $10\,\mu$s from the end mirror to the dark fringe photodiodes ($\sim 3\,$km), and negligible from the input and BS mirrors to the photodiodes (a few 10th meters) The delay appears in the overall Sc_ * _zCorr to Pr_B1_ACp delay measured in the main stream calibration.

In **Science Mode**, the ligth is stored in the Fabry-Perot cavities, with a finesse of ~ 50. The optical response for the signals from the end mirror to the dark fringe photodidoes is modeled by a simple pole with a pole of $\sim 500\,$Hz. For frequencies lower than 500 Hz, the phase is equivalent to a delay of the order of $320\,\mu$s. The pole of the cavities is taken into account in the h-reconstruction. No delay from the optical response of the interferometer should thus be taken into account in the overall Sc_ * _zCorr to Pr_B1_ACp delay added in the h-reconstruction.

4.4 Dark fringe sensing timing

From the power inpinging on the photodiodes and the Pr_B1_ACp channel stored in the DAQ, the signal goes through the following path:

- the delay in the dark fringe sensing chain: photodiode, preamplifier, demodulation with a compression filter.
- the ADC readout of the dark fringe sensing, with its anti-alias filter.
- the Pr27 process, with de-compression filter.

The signals from two photodiodes are combined in Pr27 in order to build the dark fringe signal Pr_B1_ACp: Pr_B1_d2_ACp and Pr_B1_d3_ACp.

4.4.1 Expected delay

The signal processing is shown on the figure 8.

The dark fringe analog power is measured through photodiodes. The output voltage is measured through a pre-amplifier and a demodulation board. It is then filtered through an anti-alias filter which phase below 5 kHz is equivalent to a delay of $70 - 80\,\mu$s. The signal is then read by an ADC. The signals from the photodiodes are then mixed and converted into power by the Pr process.

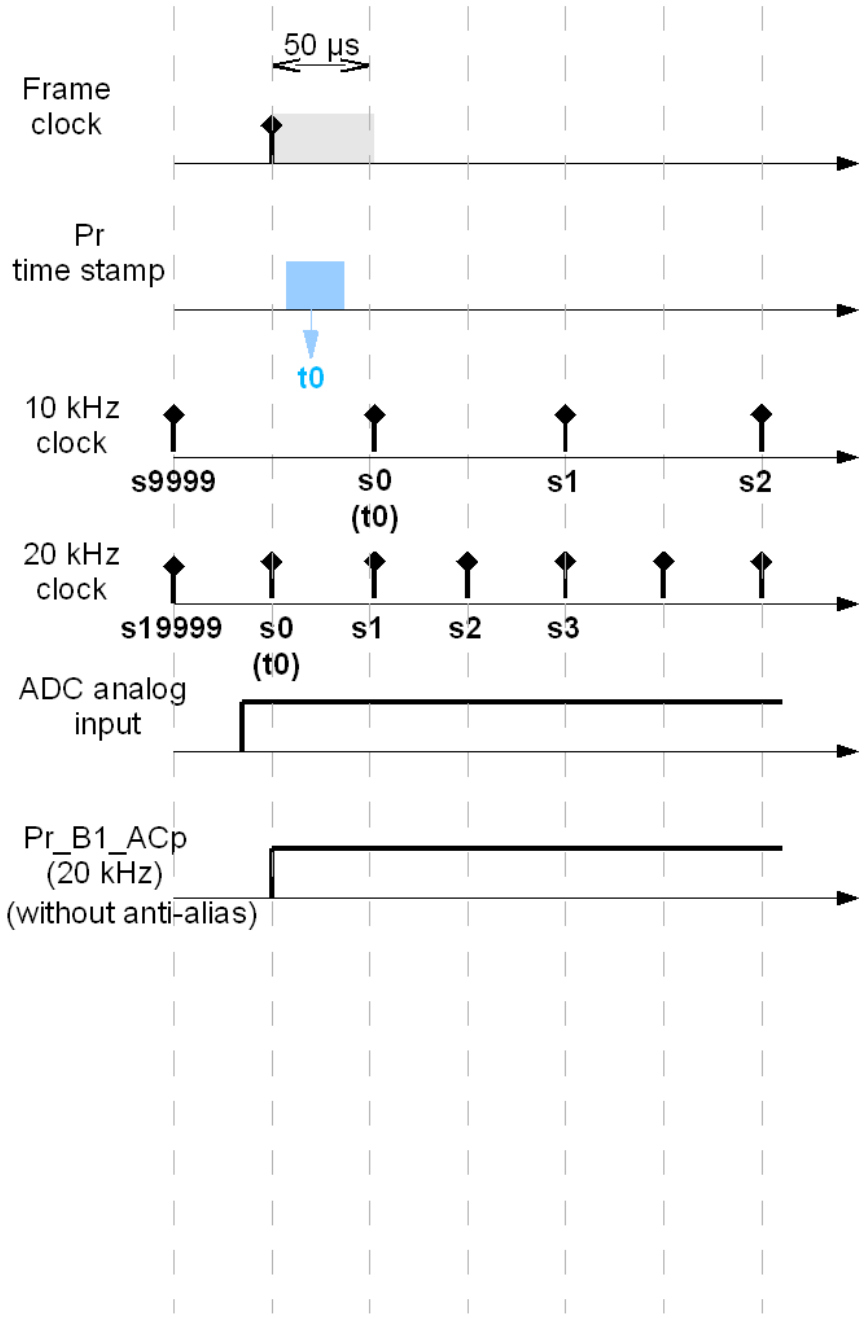

Figure 8: ***Signal processing in the dark fringe sensing part.*** *See text for details.*

The delay introduced by the photodiode/pre-amplifier/demodulation board should be lower than a few μs. The whitening/de-whitening filters are compensated in Pr27 and should not induce any delay.

The *frame signal* triggers the Pr time stamp. The Pr process has cycles at a rate of 10 kHz. The analog ADC inputs are sampled at 20 kHz and read by Pr which builds the output channel time serie Pr_B1_ACp at 20 kHz, setting the samples such that it does not introduce any delay.

The total delay introduced by the dark fringe sensing is thus the delay of the ADC anti-alias, $70 - 80\,\mu$s.

4.4.2 Measurements of the photodiode readout delay

The dark fringe channel Pr_B1_ACp is computed using the signals read from two photodiodes, Pr_B1_d2_ACp and Pr_B1_d3_ACp. The B1 compression filters located in the demodulation board have been measured in February 2007[4]. The fitted complex poles and complex zeros (with quality factor of 0.5) are given in the table 3. They have been compensated in Pr27 for every photodiode channels. These values were used during VSR1 for the compensation.

	February 2007		October 2007	
Channel	f_0 (Hz)	f_p (Hz)	f_0 (Hz)	f_p (Hz)
Pr_B1_d2_ACp	22.6	131.6	22.6	131.9
Pr_B1_d3_ACp	26.8	154.7	27.2	157.3

Table 3: ***Compression filter measurements.*** *The compensation filters set in PR27 use the values measured in February 2007. The measurements from October 2007 are used to check the stability of the compression filter during VSR1.*

The compression filters have been measured again in October 2007, during the post-VSR1 calibration shifts[5]. The fitted poles and zeros are given in the table 3. They are within 1% of the values used for the compensation in Pr27. This confirms the stability of the compression filter during VSR1.

The residuals of the compression filter non-perfect compensation are shown in the figure 9. The residuals of the compression filter compensation are within $\pm 3\%$ below 6 kHz. It has been also possible to fit the ADC anti-alias filter shapes up to 10 kHz in the data. The model uses

[4]Logbook entry 15067. Noise in injected before the demodulation board. It goes through the demodulation board, the ADC and its anti-alias and Pr27.

[5]logbook entry 18869

	Pr_B1_d2_ACp	Pr_B1_d3_ACp	Average model
f_N (Hz)	35288 ± 11	20932 ± 2	28110
f_B (Hz)	8636.1 ± 0.2	8726.1 ± 0.2	8681.1
t_d (μs)	-9.964 ± 0.002	-2.319 ± 0.003	-6.1
t_d^{equiv} (μs)	72.8	79.7	76.3

Table 4: ***Fit of the ADC anti-alias filter with a delay.*** *The anti-alias filter of both photodiode channels have been fitted with a Butterworth filter (f_B) and a notch (f_N). An additionnal delay t_d have been fitted. An average model have been derived from the results. For every filters, the phase below a few kHz is equivalent to a delay of the order of 82 μs. The overall equivalent delay induced in every channels are also given.*

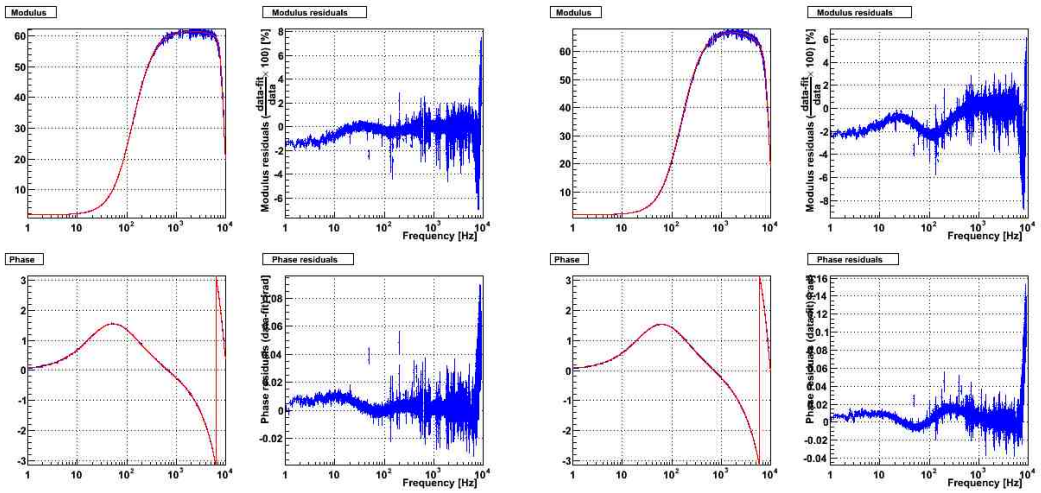

(a) Pr_B1_d2_ACp (b) Pr_B1_d3_ACp

Figure 9: ***Transfer function fits and residuals of the photodiode readout channels.*** *The measured transfer function is plotted in blue. The red curve model is the compensation filter used in Pr27 during VSR1 with an ADC anti-alias filter that have been fitted. The residuals of the fitted model are given.*

a 7th order Butterworth filter with cut-off frequency f_B and a simple notch at f_N:

$$H(\mathrm{j}f) = \frac{-\left(\left(\frac{f}{f_N}\right)^2 - 1\right)}{\left(1 + \mathrm{j}\frac{f}{f_B}\right)\prod_{k=1}^{3}\left(1 - \left(\frac{f}{f_B}\right)^2 + \mathrm{j}a_k\frac{f}{f_B}\right)} \quad (1)$$

with $a_{1,2,3} = 1.801937736,\ 1.246979604,\ 0.4450418680$.

The transfer functions are fitted from 1 Hz to 10 kHz using the points with coherence higher than 99%. The fitted parameter values are given in the table 4. The residuals are lower than $\pm 10\%$ below 10 kHz. Concerning the delay, the fitted anti-alias filters made of the Butterworth filter and of a notch have a phase equivalent to a delay of $82.4 \pm 0.4\,\mu$s below of few kHz. The global delays of the photodiode readout sensing channels (sum of the anti-alias equivalent delay and of the fitted additionnal delay) are between 72.8 and 79.7 μs respectively.

An average anti-alias filter model have been derived. It is given in the table 4. The comparison of the data and the models (specific compression filters and average anti-alias filter) as well as the residuals are given in the figure 10. The modulus residuals are still within 3% below 6 kHz but are up to 15% up to 10 kHz. The phase residuals are larger since the delays in the two channels are different but the average model uses the same value for both.

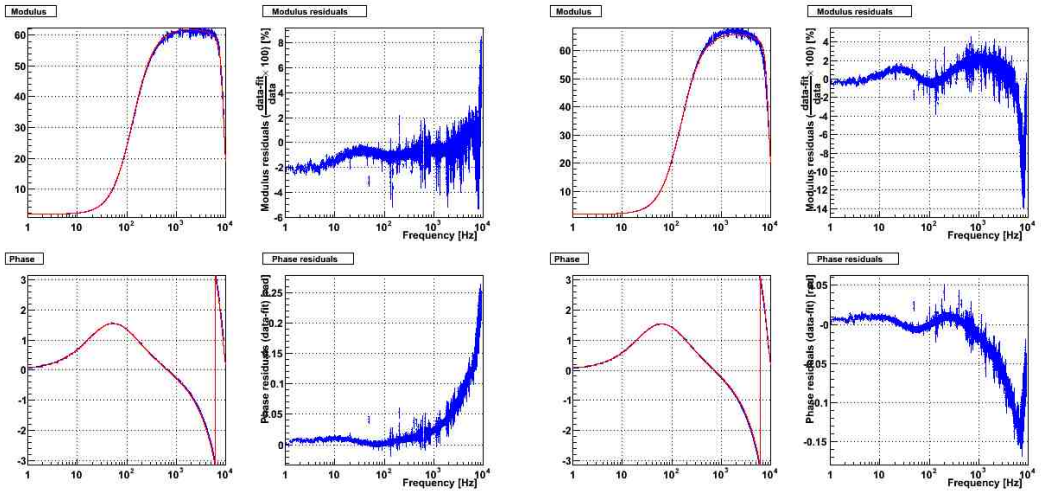

(a) Pr_B1_d2_ACp (b) Pr_B1_d3_ACp

Figure 10: ***Model with an average anti-alias and its residuals.*** *The decompression filters have been set as in Pr27. The averaged anti-alias filter described in the text have been used (Butterworth frequency, notch frequency and delay). Only the gain have been fitted.*

4.4.3 Fit of the photodiode readout transfer functions

In order to improve the model for the photodiode readout transfer functions, the data from October 2007 have been fit with a model including a gain, a delay, a complex zero, a complex pole, a Butterworth filter and a notch (8 free parameters). The fits have been computed from 1 Hz to 10 kHz using the points with a coherence higher than 99%.

The results of the fits of the transfer functions for the channels Pr_B1_d2_ACp and Pr_B1_d3_ACp are given in the table 5. The results and residuals are shown in the figure 11. The residuals are rather flat, lower than 1% in modulus and lower than 0.02 rad in phase below $\sim 6\,\mathrm{kHz}$. It could thus be useful to use such filter in the h-reconstruction and to recombine them afterwards in order to get the dark fringe signal. It would lower the signal distorsion. Also, the timing offset of the combined channels would be lower.

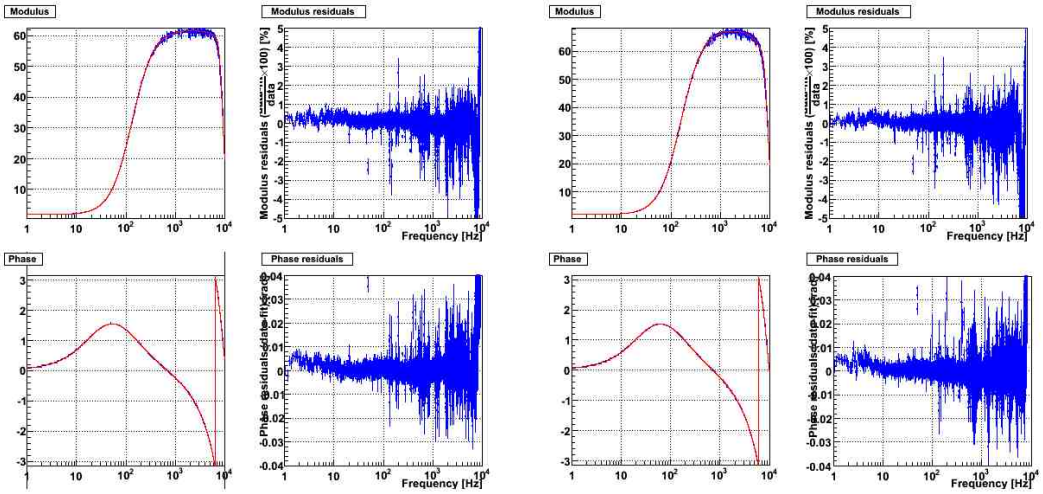

(a) Pr_B1_d2_ACp (b) Pr_B1_d3_ACp

Figure 11: ***Results of the fit of the two dark fringe photodiode readout channel transfer functions*** *with the 8-parameter model. The residuals are also given.*

4.4.4 Conclusion

The measurements of the delay induced in the photodiode readout channels are in agreement with the expected values, between 70 and 80 μs. However, a difference of 7 μs is found between the two channels that are combined to compute the dark fringe channel Pr_B1_ACp. These are systematic errors on the Pr_B1_ACp channel timing. It is possible to reduce this error recombining the photodiode signals offline, applying the model including the anti-alias filter fits.

	Pr_B1_d2_ACp	Pr_B1_d3_ACp
Gain	1.79879 ± 0.00028	1.98613 ± 0.00028
Delay μs	-9.7965 ± 0.0025	-1.7009 ± 0.0027
f_0 (Hz)	22.364 ± 0.002	26.8008 ± 0.0025
Q_0	0.49790 ± 0.00009	0.491723 ± 0.000085
f_p (Hz)	131.39 ± 0.01	157.021 ± 0.015
Q_p	0.49544 ± 0.00004	0.492754 ± 0.000038
f_B (Hz)	8648.35 ± 0.20	8773.09 ± 0.23
f_N (Hz)	34096 ± 11	20077 ± 2.17

Table 5: ***Results of the fit of the two dark fringe photodiode readout channel transfer functions*** *with the 8-parameter model.*

4.5 Summary

The summary of the expected delay from Sc_ $*$ _zCorr to Pr_B1_ACp for the end mirrors is shown in the figure 12 in the case of free Michelson data in LN mode.

The expected delay for free Michelson data in LN mode are summarized in the table 6 and compared to the delay measured from the calibration main stream. For the end mirrors, the measured delay is compatible with the expected one. However, the delay measured in this note between the current flowing in the coil and Sc_ $*$ _zCorr channel is 20 μs lower than expected.

For the BS mirror actuation channels, the measured delay are different from a channel to another, within $\sim 40\,\mu$s from the expected one.

Such difference can be used as a systematic error in the delay measurements.

Delay origin	From NE, WE	From BS
Coil actuation	331	333
Mirror deformation	30	20
Light propagation	10	0
Dark fringe sensing	$70 - 80$	$70 - 80$
Total expected delay	$441 - 451$	$423 - 433$
Calibration delay	451 ± 3	400 ± 1

Table 6: ***Summary of the expected delays (in μs) from the mirror actuation (LN mode) to the dark fringe readout.*** *The delay measured in the calibration main stream is also given for comparison.*

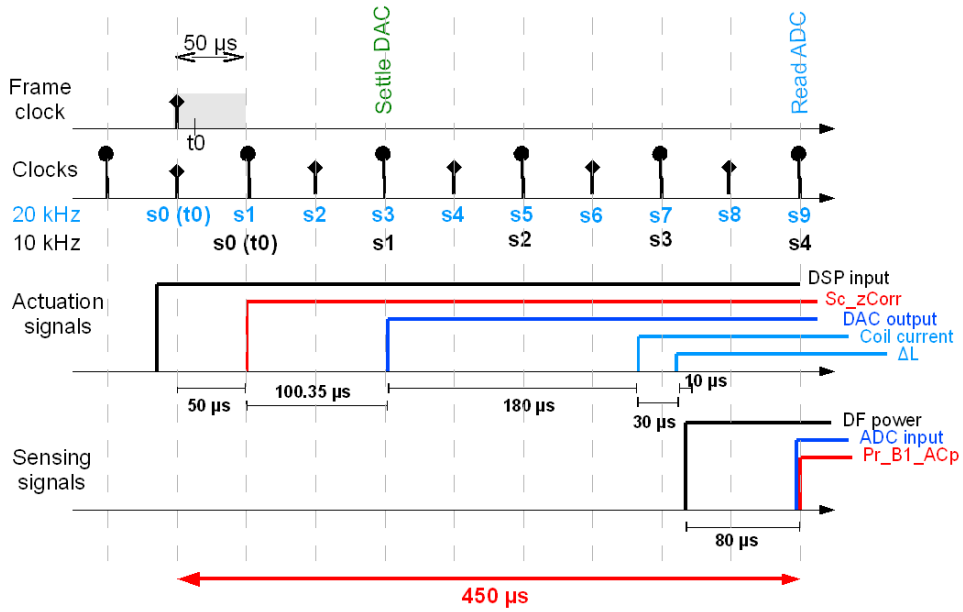

Figure 12: ***Signal processing from*** Sc_ ∗ _zCorr ***to*** Pr_B1_ACp *See text for details.* d_1 *is the DAC settling time of* 0.35 μs.

5 Checks of the Virgo timing system stability

5.1 Timing jitter

A spectrum of the jitter of the timing system has been measured in April 2008 (see logbook entries 20292 and 20293). The 10 MHz signal from the atomic clock is used as a reference signal that is compared to one of the signals used by the timing system, the 2.5 MHz so called *fast clock* signal.

A first measurement of the signal using an oscilloscope shows an RMS of about 200 ns (integrated over many seconds). This is consistent with the observed RMS of ~ 200 ns for the propagation time to each building measured using two different GPS receivers (the TiM_rtt$\{1,2,3,4\}$ signals), measurement limited by the 100 ns resolution of the GPS receivers.

The comparison of the signals produced simultaneously by two timing boards, or by the propagation trough 3 km of optical fibers gives an RMS less than 0.2 ns. This means that the jitter introduced by the timing distribution is much smaller than the one of the GPS receiver.

To get a spectrum of the overall timing jitter and therefore validate this hypothesis, the 2.5 MHz signal was mixed with the 10 MHz signal using a demodulation board (B1_d7) and acquired in phase and quadrature (the compression filters have been compensated for). The phase and quadrature signal gives a measurement of the relative dephasing of the two signals at 10 MHz. Integrating this phase, the time difference between the two clocks, and therefore the jitter of the timing distribution, can be reconstructed.

The figure 13 shows the spectrum of this signal. Above one 1 Hz, the estimated time jitter is below 1 ns/$\sqrt{\text{Hz}}$. At low frequency there is a bump corresponding to the 200 ns previously observed RMS.

5.2 Absolute time variations during VSR1

The monitoring signals TiM_GTimeN and TiM_rtt$\{1,2,3,4\}$ of the timing system during VSR1 are shown in figure 3.

The delay between the master timing clocks and the GPS receiver clock changed from 2.7 to 2.3 μs on August 3rd 2007, around 14h18m42s UTC.

The RMS of the TiM_rtt$\{1,2,3,4\}$ during VSR1 are of the order of 200 ns, negligible compared to the propagation delay of 34.1 μs.

An independent atomic clock is used to check that there is no glitches in the Virgo timing system. The 1 PPS signal from the atomic clock is converted into a ramp (as described in 3.1.2 (p. 5)), sampled through a 16-channels ADC and stored in the DAQ. A fit of the ramp is performed online in order to estimate the delay between the 1 PPS and the frame clock. The delay is saved in the channel TiMoni_Ti_AtomicPulse_t0 in secondes. Its evolution during VSR1 is shown in the figure 14(a). The atomic clock is more stable than the clock from the GPS receiver at short term, but derives at longer term compared to the reference GPS time.

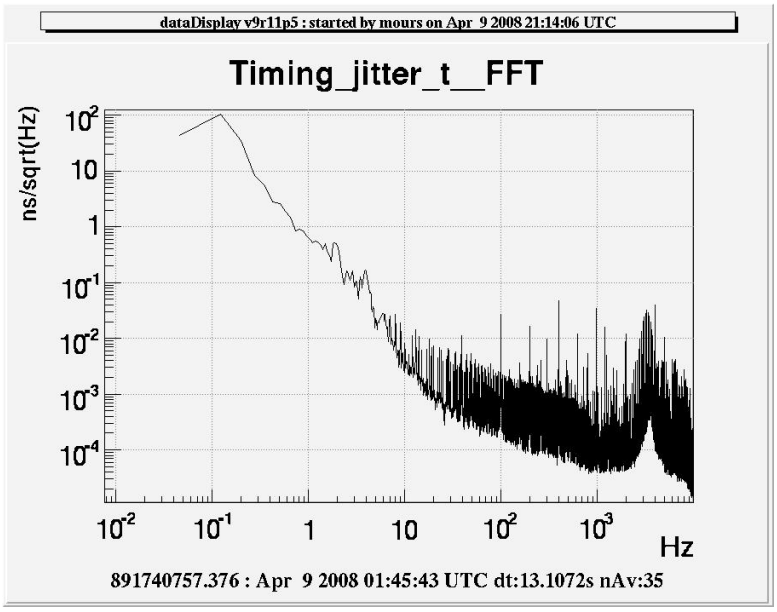

Figure 13: ***Spectrum of the jitter of the timing system.***

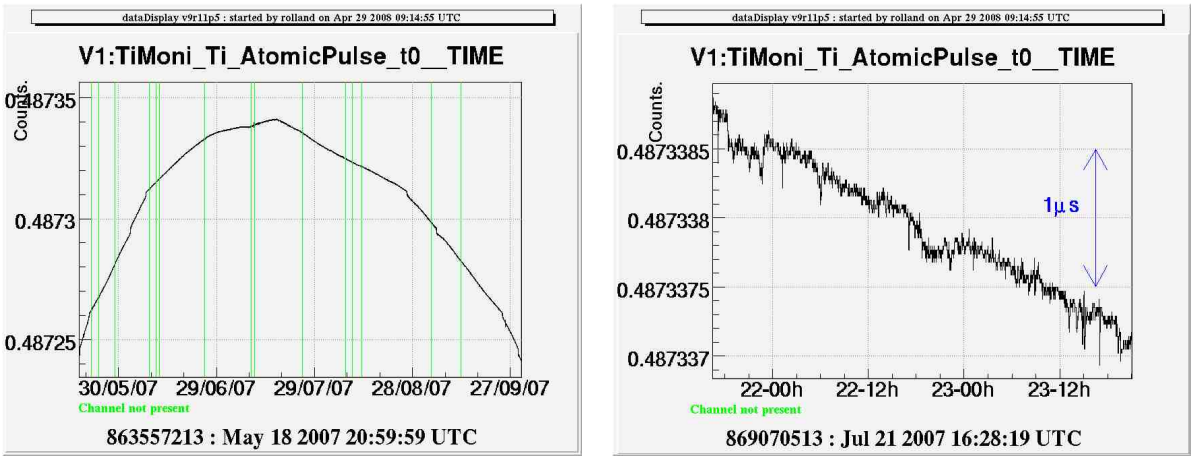

(a) VSR1 monitoring.

(b) 2 days monitoring.

Figure 14: ***Monitoring of the channel*** TiMoni_Ti_AtomicPulse$_t$0 ***during VSR1 and estimation of the signal width.***

An estimation of the short term error of the Virgo timing system is given by the width of the signal corrected for the long term deviation. The error can be estimated from figure 14(b) to be less than 1 μs.

6 Conclusions

The absolute timing of the Virgo data have been measured. During VSR1, a delay of 21 μs have been estimated for the dark fringe signal time-serie, with a systematic error of the order of 2 μs. The Virgo time jitter has been estimated to be lower than 200 ns.

The two photodiode readout channels that are used to compute the dark fringe channel Pr_B1_ACp have been characterized up to $\sim$ 10 kHz. An additionnal systematic error of 7 μs on the Pr_B1_ACp timing has to be added since the measured delays are different between the two channels.

The delay from the Sc_ $*$ _zCorr channels in LN mode to the dark fringe channel Pr_B1_ACp has been estimated from the different pieces of the chain. They are in agreement with the delays measured by the calibration main stream within 40 μs. The difference is not understood. This gives the order of the tuning of the delays that could be done to combine the actuation signals and the dark fringe signal in the h-reconstruction. This error can also be used as an upper limits on the systematic error of the dark fringe timing coming from our understanding of the overall calibration chain. This would include the 7 μs found above.

In conclusion, the systematic errors of the dark fringe absolute timing, after correction of the Virgo absolute time offset, are estimated to the order of 40 μs.

References

[1] A. Masserot et al. (VIRGO collaboration), *The Virgo Data Acquisition System* (2003) Proc. of the 13th IEEE NPSS Real Time Conference, Montreal, Canada (Virgo note LAPP-EXP-2003-12).

[2] L. Rolland, F. Marion, B. Mours *Mirror and marionette actuation calibration for VSR1* (2008) VIR-015A-08.

[3] P. Puppo, *A finite element model of the Virgo mirrors* (2004) VIR-NOT-ROM-1390-262.